Ab initio atomistic description of temperature-induced phase changes: The cases of zirconia and Ti-Y-co-doped zirconia

Fabio Negreiros Ribeiro [*]

Centro de Ciências Naturais e Humanas, Universidade Federal do ABC, Santo André, SP, Brazil
and INFIQC, CONICET, Departamento de Química Teórica y Computacional, Facultad de Ciencias Químicas,
Universidad Nacional de Córdoba, Argentina

Dolores Ribeiro Ricci Lazar , Valter Ussui , and Nelson Batista de Lima
Centro de Ciência e Tecnologia de Materiais (CECTM) do Instituto de Pesquisas Energéticas e Nucleares, SP, Brazil

Juliana Marchi and Gustavo Martini Dalpian
Centro de Ciências Naturais e Humanas, Universidade Federal do ABC, Santo André, SP, Brazil

Zirconium dioxide, or zirconia, is a common and useful ceramic with a wide range of applications, from fuel cells to odontology. Its phase diagram is simple and well understood, having a structure which is monoclinic at temperatures up to 1500 K, tetragonal up to 2700 K and cubic up to 3000 K. Zirconia is rarely used in its pure form, being typically doped with Y_2O_3, MgO or TiO_2, and in this regime its phase diagram becomes much more complex. In this context, *ab initio* molecular dynamics (AIMD) can provide a detailed atomistic description of the phase diagram of this system, accurately describing its stable phases and transition regions. In this work, 3 mol-% Y_2O_3 (3YSZ) crystals doped with different Ti contents were studied at the density-functional level. For Ti contents varying from 0 to 30 at%, a global search algorithm was first used to explore the 0 K potential-energy surface and determine the most stable sites for the added Ti atoms. It was found that, at low Ti compositions X_{Ti}, small TiO_2 clusters form, followed by TiO_2 channels and infinite TiO_2 planes at larger X_{Ti} values, and that the highest stability is achieved at 9% Ti. AIMD simulations within the isothermal-isobaric NPT ensemble were then performed to characterize the temperature-dependent phase changes as a function of the Ti content, where it was found that the Ti-doped structures presented considerably smaller volume changes near the phase-change critical temperatures. These findings suggest that YSZ materials doped with a small amount of Ti are both energetically and kinetically more stable than the undoped counterparts, in the ideal proportion of 3% TiO_2 for every 1% Y_2O_3 doping.

I. INTRODUCTION

Zirconium dioxide, or zirconia, is a ceramic with a high melting temperature, excellent oxygen mobility, and low electronic and thermal conductivity. These properties make such a material very useful in a wide range of applications, from odontology, as the main material composing tooth crowns, to thermal barrier coatings in gas turbines [1]. Even though zirconia is an important ceramic material, it presents phase transitions when submitted to large temperature changes. It can, in fact, crack when cooled from high temperatures due to a transition from the metastable tetragonal (Tet) phase to the most stable and also 5% greater volume monoclinic (MC) phase [1]. Therefore, in most applications zirconia is doped with other oxides in order to optimize its properties. Zirconia is typically doped with Y by mixing ZrO_2 with Y_2O_3, forming yttria-stabilized zirconia (YSZ), which creates oxygen vacancies that end up stabilizing the tetragonal and cubic (Tet and

Cub) symmetries over the MC symmetry, mostly due to the reduced amount of oxygen [1,2]. TiO_2, or titania, is another dopant that has also been shown to stabilize the Tet phase [3], connected to the changes brought by Ti that make the MC volume and atomic positions similar to the tetragonal positions, nearing their differences and lowering the transition temperature between the phases. Several studies on the Y-Ti codoped zirconia material can be found in the literature [4–9]. In particular, Zeng *et al.* [4] reported that 3 mol% yttria-stabilized zirconia (3YSZ) micropillars doped with 5 mol% Ti were much larger in size after being sintered at high temperatures compared with the Ti-free counterparts and also presented shape memory effects.

From the simulation point of view, zirconia and YSZ crystals have been extensively studied in the past. Ti doped zirconia has also been considered in the literature [10,11], however in more limited contexts. In most works, standard density-functional calculations [12] within the local density (LDA) and/or gradient corrected (GGA) functionals were performed [13–20]. In terms of the 0 K equilibrium structural parameters, both LDA and GGA offer a very good

---
[*]fabio.ribeiro@unc.edu.ar

structural description of all the phases of this system, showing deviations of at most 2% compared with the experimentally predicted data [18]. However, LDA underestimates, while GGA overestimates the stability, in terms of energy, of the MC phase with respect to the Tet phase [16,18], therefore predicting that the transition MC-Tet occurs at lower or higher temperatures than the experimental ones. Furthermore, Jomard *et al.* [21] have shown that gradient corrections are required for an accurate description of zirconia's orthorhombic structure at high pressures, even though there is an overall loss of agreement compared with experimental results for some of the compared structural properties. Considering these aspects, GGA functionals should offer, in principle, a suitable structural description of the system while keeping the computational cost to a minimum, at least compared with newer functionals or approaches that are usually more expensive, yet potentially more accurate.

To the best of the authors' knowledge, Y-Ti codoping of zirconia was rarely atomically characterized in depth [22], especially taking into account all the different phases it can present, the distinct Ti contents, and also the high temperatures these systems are usually submitted to. In fact, kinetic phase changes due to temperature are usually not simulated at all at the *ab initio* level, due to their significant complexity and computational cost. However, they can provide important information regarding the phase diagram of a specific system, with an atomistic description at each composition and temperature under consideration.

From the experimental perspective, x-ray diffraction (XRD) is the standard technique used to accurately determine the lattice parameters and symmetry of crystals. However, it gives a structure averaged over several unit cells, over both time and space, which might hinder local and instantaneous effects. Pair distribution function (PDF) measurements are usually able to observe the short-range order in materials. This has been recently noticed in halide perovskites [23–26] regarding the precise structural details of their cubic phases. By computer simulation, on the other hand, it is possible to successfully investigate the structural changes resulting from local atomic variations and how they affect the material as a whole. In the light of these issues, molecular dynamics appears as a powerful tool to provide an accurate quantitative description of a crystal structure. Dynamics at constant number of molecules, pressure, and temperature (NPT ensemble), in particular, can take into account atomic vibrations, atomic diffusion, and unit-cell changes simultaneously, allowing the study of phase transformations.

The main objectives of this work are twofold. We first made an atomistic study of the phase diagram of zirconia, considering the different phases it can present and also analyzing the effects of temperature, in a wide range from room to melting temperatures. Since large amounts of Y make the tetragonal or cubic phases much more stable than the monoclinic one, therefore nearly eliminating the interesting MC → Tet transition, we considered a very small amount of Y doping, studying the effect of increasing amounts of Ti on the system's properties. For this, we performed a theoretical study at the DFT-GGA level to determine the structural changes of 3YSZ when doped with 0% to about 30% of Ti. A global search approach was first applied to find that, as Ti content increases,

Ti goes from forming small TiO_2 clusters inside the 3YSZ structure, to TiO_2 channels, and then infinite TiO_2 planes. The main difference between the MC and Tet phases is shown to be progressively smaller, too. Furthermore, the lowest formation energy (maximum stability) was found at the special concentration of 9 mol%, and at temperatures between 1100 and 1500 K, the common temperatures at which this material is usually treated, the decrease in volume due to the MC → Tet transition was found to be smaller for the Ti-doped structures, resulting in a larger resistance to cracking.

The second objective was to assess the accuracy and limitations of *ab initio* molecular dynamics (AIMD) within the NPT ensemble. Since this approach is not often used to study phase diagrams, due to its cost and not-so-straightforward application, a detailed analysis was performed for the system in question. The NPT-AIMD approach was shown to give an accurate description over the whole temperature range, even at temperatures as high as 2750 K and at the more complex phase-transition regions.

II. COMPUTATIONAL DETAILS

All calculations were performed at the density-functional (DFT) level [12] with the Perdew-Burke-Ernzerhof [27] exchange-correlation functional. For the global search and dynamics parts, the CP2K software [28] was used with the pseudopotentials of Goedecker, Teter, and Hutter with 1, 6, 16 electrons for H, O, Fe [29–31], respectively, and the double-zeta valence plus polarization Gaussian basis function (DVZP) [32]. An energy threshold for self-consistency of 1×10^{-7} a.u. and cutoffs of 600 (50) Ryd for the finest grid (relative grid) for Gaussian mapping were adopted, respectively. The most stable 0 K structures found were re-optimized with a higher accuracy with the QUANTUM ESPRESSO (QE) software [33], using the GBRV pseudopotentials [34], a $2 \times 2 \times 2$ Monkhorst-Pack *k*-point sampling [35], a 1×10^{-7} a.u. energy threshold for self-consistency and 1×10^{-5} (1×10^{-4}) a.u. energy (force) thresholds for geometry optimization. The variable-cell optimization was applied without constraints, if not explicitly stated otherwise.

The $2 \times 2 \times 2$ supercell containing 32 ZrO_2 units is the starting point of all structures studied in this work. 3% Y doping was achieved by replacing two Zr by two Y atoms, also adding an oxygen vacancy to keep charge neutrality, as done in similar works [14–19]. Ti doping consisted in a direct substitution of 1 Zr by 1 Ti atom. To determine the most stable sites for Ti doping starting with the supercell illustrated in Fig. 1(b), we applied the basin hopping (BH) global search [36] algorithm, which provides a cheap and fairly accurate way to explore an unknown potential-energy surface. We have used a homemade code that externally calls the CP2K software every time a geometry optimization is required. Each step of the algorithm consists in (1) exchange a Ti with a Zr atom; (2) perform a geometry re-optimization; (3) evaluate the energy change ΔE with respect to the previous configuration; (4) accept the atomic exchange following the Metropolis criteria, i.e., with a 100% probability if the new structure is more stable ($\Delta E < 0$), or with a $e^{-\Delta E/KT_f}$ probability otherwise, where K is the Boltzmann constant and T_f is a fictitious temperature. This is repeated N_S times, until no
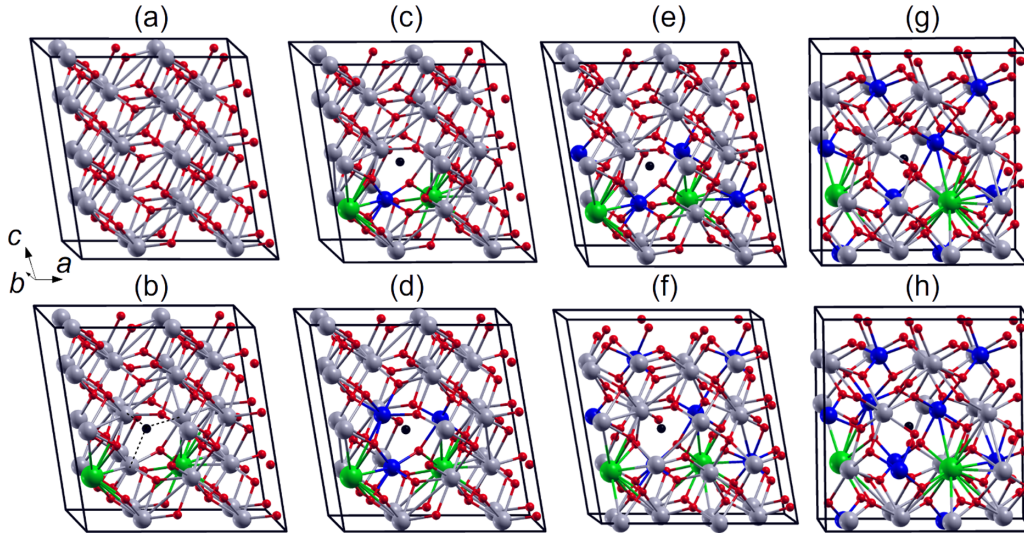
FIG. 1. Panels (a) and (b) show the MC unit cell for the pristine ZrO$_2$ structure and the 3%-Y doped (3YSZ) configurations, respectively. The most stable minimum found for the Ti-doped 3YSZ structure at Ti compositions of 3%, 6%, 13%, 19%, 25%, and 31% are shown in panels (c)–(h), respectively. Zr, O, Y, and Ti atoms are in gray, red, green, and blue, respectively, and the oxygen vacancy is illustrated with a black sphere.

new structures are generated for a few hundred steps. In this work, each BH run was performed with $T_f = 150$ K and N_S between 500 (6% Ti doping) and 2000 steps (30% Ti doping).

Ab initio molecular dynamics (AIMD) simulations were performed starting from the 0 K most stable structures at each chemical composition, as illustrated in Fig. 1. A NPT ensemble was used with a time step of 1 fs (0.5 fs for temperatures larger than 2000 K), a 100 fs time constant for temperature control, a 75 fs time constant for pressure control, a target pressure of zero GPa, and 15 target temperatures: 250, 500, 750, 1000, 1125, 1250, 1375, 1500, 1625, 1750, 1875, 2000, 2250, 2450, and 2750 K. The total time of each run was 40 ps, where the first 25 ps were taken as a thermalization time, being discarded in the averages performed. The total potential plus kinetic energy and the pressure as a function of the simulation time for the pure zirconia crystals at several different temperatures are presented in the supplemental material [37], which show that the total energy is stabilized after 25 ps, while the pressure converges to zero much more quickly.

III. RESULTS AND DISCUSSION

A. Zero kelvin analysis

Our starting point was the pristine ZrO$_2$ supercell composed of 32ZrO$_2$ units arranged in a tetragonal phase (other phases will be considered later), as illustrated in Fig. 1(a). 3%-Y doping was achieved by replacing two Zr atoms with Y, adding also an oxygen vacancy (O$_v$) to guaranty charge neutrality, as illustrated in Fig. 1(b). A 1000 steps global search for the best position of the Y atoms with respect to the fixed O$_v$ position was performed. In parallel, a complete search considering all possible 32×31 distinct configurations was also done so as to determine the optimized value for the fictitious temperature of the BH approach that generates all the most stable structures with the lowest number of steps. It was found that the most stable configuration corresponds to both Y atoms being second neighbor to O$_v$ and also third

neighbor to each other, as illustrated in Fig. 1(b). There were, however, many other nearly degenerate configurations, related to Y-Y second or fourth neighbor to each other, but always surrounding O$_v$. Only when the Y atoms are close to each other or far from the O$_v$ does one get a significant increase in energy of at least +5 meV/ZrO$_2$. This is in agreement with what has been already obtained and discussed in the literature [14–16]. Therefore, in the search performed next for the best chemical configurations for Ti, the positions of the Y atoms in the unit cell were fixed in the most stable position determined [Fig. 1(b)].

Ti doping of the 3YSZ structure consisted in a direct substitution of Zr by Ti. Each added Ti corresponds approximately to 3.1% to the Ti composition within the cell (X_{Ti}), and the X_{Ti} range considered was 0% to 31%. The most stable structures obtained following the BH global search approach are shown in Figs. 1(c)–1(h). Three distinct chemical regions can be identified from this figure. At low compositions ($X_{Ti} < 10\%$), the Ti atoms are preferentially located as first neighbor to the oxygen vacancy (O$_v$), in one of the three first-neighbor sites that are at a distance shorter than 2.6 Å, illustrated with dashed lines in Fig. 1(b). The first occupied site is preferentially the site also first neighbor to a Y atom [Fig. 1(c)], and eventually all three sites are occupied at $X_{Ti} = 9\%$ [Fig. 1(d)]. This can be understood by considering that the Ti coordination in the standard rutile or anatase TiO$_2$ phases is six, with a Ti-O bond length of about 1.95 Å, while in the MC ZrO$_2$ structure these values are 7 and 2.15 Å, respectively. Therefore, the sites closer to the O$_v$ offer a better strain release for Ti. For compositions in the $10\% < X_{Ti} < 20\%$ range, we note the formation of TiO$_2$ channels [see Fig. 1(e)] tangent to the oxygen vacancy. This Ti channel can point in both the [100] or [010] directions, with nearly zero energy difference between each case. However, when aligned in the longer [001] or [110] directions, one gets a total-energy increase of at least +4 meV/ZrO$_2$. For $X_{Ti} = 25\%$, a TiO$_2$ plane is formed, [Fig. 1(g)], with a normal vector that can point in either the
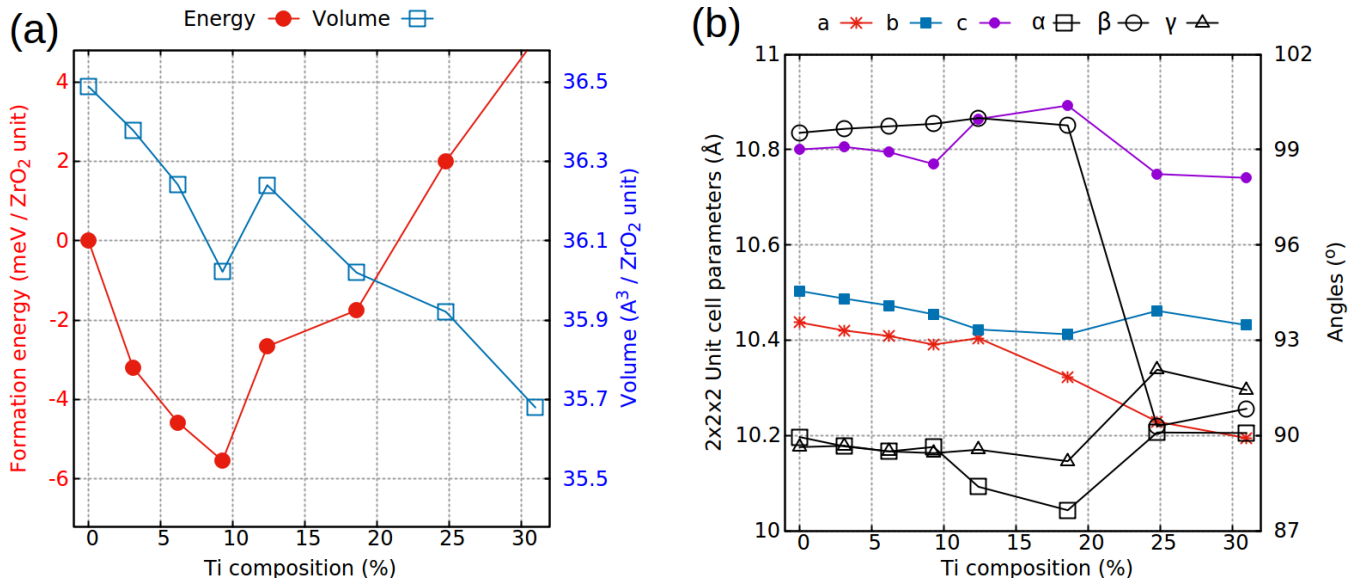
FIG. 2. Panel (a) shows 0 K formation energy (in meV/ZrO$_2$ unit) and volume (in Å^3/ZrO$_2$ unit) of the most stable 3YSZ structures found at different Ti compositions. Panel (b) shows the optimized unit-cell parameters (vector lengths and angles) for each case.

[100] or [010] directions. Finally, for higher coverage (25% < X_{Ti} < 32%), the additional Ti atoms locate in sites far from the Ti plane, preferentially maximizing the interaction with Y instead, and far from the vacancy [Fig. 1(h)].

In Fig. 2(a) we show the formation energy ΔH and unit-cell volume per ZrO$_2$ unit (for a total of 32) as a function of X_{Ti} for each structure illustrated in Fig. 1. To focus on the energy changes due to Ti doping only, ΔH was evaluated with respect to the 3YSZ structure and taking as reference the orthorhombic zirconium titanate structure (ZrTiO$_4$) [38], such that

$$\Delta H = E^{tot} - E^{3YSZ} - N_{Ti}[E^{ZrTiO_4} - 2E^{ZrO_2}],$$

where E^{tot}, E^{3YSZ}, E^{ZrTiO_4}, and E^{ZrO_2} are the total energy, the energy of the undoped 3YSZ, of the orthorhombic ZrTiO$_4$ and MC ZrO$_2$ structures, respectively, and N_{Ti} is the number of doping Ti atoms. Figure 2(a) reveals that the formation energy decreases almost linearly up to $X_{Ti} = 9\%$, reaching a minimum at this value. This composition corresponds to an O$_v$ site completely surrounded by Ti, as illustrated in Fig. 1(d). Even more interestingly, the volume also shows a clear minimum at this point, which suggest that that there is a reduction in the volume due to Ti–O bonds being smaller, but there is also an additional electrostatic effect around the oxygen vacancy, which further reduces the volume. For $X_{Ti} = 12\%$, when TiO$_2$ channels form, we get a significant increase in both enthalpy and volume. Indeed, at this composition we note a large number of minima very close in energy and with similar volumes, but with very different chemical arrangements (see Fig. S1 of the supplemental material [37]), which means that this concentration is in a metastable chemical point, where there is too much Ti for the number of oxygen vacancies and too little Ti to form extended TiO$_2$ rows or planes. At larger X_{Ti} values, the energy (volume) linearly increase (decrease) up to $X_{Ti} \approx 22\%$, where the enthalpy becomes positive. At this point, phase separation becomes favorable, with the formation of both zirconium titanate ZrTiO$_4$ and 3YSZ with low Ti

content. This is in agreement with the reported phase diagrams for the binary ZrO$_2$-TiO$_2$ system [6].

In Fig. 2(b) the variation of the supercell parameters with X_{Ti} are shown. It can be seen that the Ti-doped 3YSZ structure is nearly MC at lower compositions (0% < X_{Ti} < 10%), where Ti addition causes just a large compression on both a and b lattice vectors, with a much smaller reduction on the "c" vector. This overall homogeneous reduction is expected since the Ti atoms are locally surrounding the O$_v$ site, and no rows or planes are formed. At 10% < X_{Ti} < 20%, a large expansion in the c direction is obtained with a structural rearrangement in the planar "ab" region. This means that, because Ti-O bonds are shorter than Zr-O bonds, it is energetically more stable to strengthen the Ti-O planar interactions and release the strain caused on the Zr-O bonds by increasing the perpendicular size of the unit cell. This competition is the main reason for the increased volume in this intermediate region shown in Fig. 2(a). At $X_{Ti} > 24\%$, after a complete Ti plane is formed, we get a nearly MC to nearly orthorhombic transformation, and a large decrease in the c vector, since now a much better strain release can be accomplished. The decreased stability of the MC structures could be expected given the orthorhombic symmetry of the known stable ZrTiO$_4$ structure. We also point out that the sudden change in the β angle at $X_{Ti} > 24\%$ is in agreement with x-ray diffraction experiments in zirconia doped with TiO$_2$, where it is observed that, at room temperatures, where typically MC phases are obtained, a tetragonal Zr$_3$TiO$_8$ phase can be stabilized in slow-cooling conditions with about 25% Ti doping [3].

As mentioned in the introduction, even though the Tet and Cub phases are metastable at 0 K, at larger temperatures they become more stable than the MC phase, and the transitions MC → Tet and Tet → Cub are expected. We add that, for Ti contents higher than 9%, there is loss of symmetry due to the formation of Ti channels or planes, and the 0 K MC phase becomes actually triclinic (however, very close to a MC structure), while the tetragonal becomes orthorhombic (again
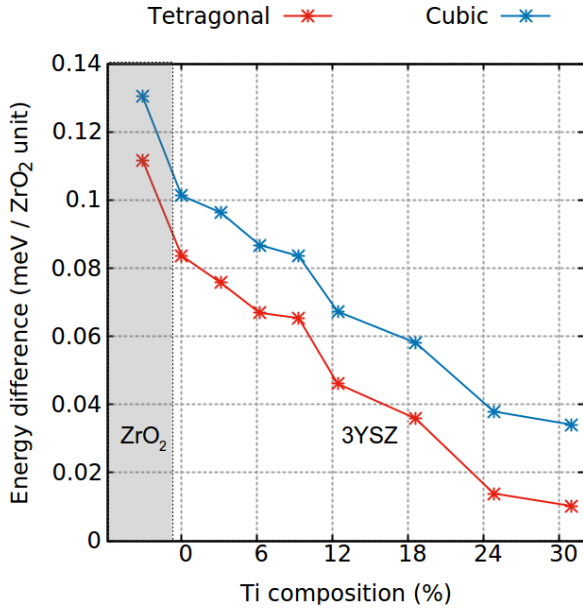
FIG. 3. Energy difference between the most stable monoclinic (or nearly monoclinic) phase and the tetragonal (in red) and cubic (in blue) phases for the 3YSZ material with different Ti compositions, from 0% to 31%. The points behind the dashed transparent rectangle show the values for the pristine ZrO_2 crystal, as a reference.

very close to tetragonal). So for the following analysis we consider the triclinic phases as near MC and the orthorhombic phases near Tet. One way to estimate these transitions at 0 K is by constraining each symmetry during the structural optimization, and then comparing their energies. The energy differences obtained are shown in Fig. 3, taking as zero-energy reference the MC case, or triclinic. From the plot we first note that Y doping significantly stabilizes the Tet and Cub phases. Ti doping, similarly, also stabilizes these phases, although less efficiently than Y, which is in agreement with experimental results from the literature [1]. Furthermore, the energy difference between Tet and Cub phases also increases with Ti content, which is in agreement with the common knowledge on the ZrO_2-TiO_2 binary system where the cubic phase is overall not stable at temperatures below 2600 K for nearly all Ti compositions [6].

Static calculations give an important starting point to understand the stability of different configurations and phases, but they have two drawbacks: First, they are limited by the different geometries and phases considered. Second, they lack kinetic effects that could be extremely important depending on the conditions a material is submitted to. Indeed, such a limitation is a problem in the case of stabilized zirconia, typically involved in experiments at high temperatures between 1000 to 2500 K, where harmonic approximations are, in general, not valid or too inaccurate. Thus, we study next the kinetic properties of this system by doing molecular dynamics within the NPT ensemble.

B. Kinetics of ZrO_2

Pristine ZrO_2 has a very well characterized phase diagram [6,39]. It is monoclinic at temperatures below 1500 K, tetragonal between 1500 and 2700 K, and cubic from 2700 to 3000 K, melting at higher temperatures. Previous works have provided an atomic characterization of each phase, but the actual path connecting different structures during a phase transformation is only rarely studied [40]. Therefore, before studying the Ti-doped 3YSZ material, we performed a detailed study of pure zirconia, analyzing both the transition regions and the kinetic stability of each phase.

The main approach consisted in performing several constant-pressure and -temperature (NPT) *ab initio* molecular-dynamics runs at different temperatures. This NPT-AIMD approach can, in principle, provide an accurate quantitative description of the structural properties and phase changes of the target system for a wide temperature range, from 0 K to the system's melting point. Since NPT ensembles can allow changes in the system's volume, and given that volume changes might cause numerical instabilities at the DFT level for periodic systems and plane-wave basis sets, the dynamics results shown next also have the purpose of checking the overall accuracy of our approach.

NPT-AIMD runs were performed at temperatures in the range 500 K $< T <$ 2750 K. In Fig. 4(a) the average supercell volume as a function of the simulation time is shown for a few chosen T values, where it is clear that the average volume quickly stabilizes after only a few picoseconds for $T < 1500$ K, and an accurate average value can be obtained with an integration over a short 5–10 ps interval. Plotting the supercell parameters (lengths and angles) as a function of time for the 500 K case, for example [in Fig. 4(b)], one can see a rather straightforward picture for the whole run: the cell symmetry is monoclinic at each time step, with $a \neq b \neq c$ and $\alpha = \gamma \approx 90°$ and $\beta \approx 99°$. We further note that increasing

TABLE I. For the AIMD runs of pure zirconia at different target temperatures T_{trg}, we show the following averages and their respective deviations: temperature (T_{avg}), supercell angles (α, β, γ), supercell ratios b/a and c/a, and volume per ZrO_2 unit (V_{avg}).

| T_{trg} (K)	T_{avg} (K)	V_{avg} (Å^3)	b/a	c/a	α (°)	β (°)	γ (°)
500	501 $\pm$ 32	36.5 $\pm$ 0.2	1.007 $\pm$ 0.007	1.037 $\pm$ 0.006	90.0 $\pm$ 0.3	99.4 $\pm$ 0.5	90.0 $\pm$ 0.2
1175	1187 $\pm$ 76	37.3 $\pm$ 0.3	1.00 $\pm$ 0.01	1.04 $\pm$ 0.01	90.0 $\pm$ 0.5	98.7 $\pm$ 0.8	90.0 $\pm$ 0.5
1350	1363 $\pm$ 88	37.5 $\pm$ 0.3	1.00 $\pm$ 0.01	1.04 $\pm$ 0.01	90.0 $\pm$ 0.6	98.3 $\pm$ 0.9	90.0 $\pm$ 0.4
1500	1510 $\pm$ 99	37.4 $\pm$ 0.4	1.00 $\pm$ 0.01	1.04 $\pm$ 0.01	90.0 $\pm$ 0.7	91 $\pm$ 7	90.0 $\pm$ 0.5
1750	1747 $\pm$ 113	37.4 $\pm$ 0.4	1.00 $\pm$ 0.01	1.04 $\pm$ 0.01	90 $\pm$ 1	91 $\pm$ 1	90 $\pm$ 1
2000	2002 $\pm$ 133	37.8 $\pm$ 0.4	1.00 $\pm$ 0.02	1.03 $\pm$ 0.02	90 $\pm$ 1	90 $\pm$ 1	90 $\pm$ 1
2350	2382 $\pm$ 159	38.3 $\pm$ 0.5	1.00 $\pm$ 0.03	1.01 $\pm$ 0.03	90 $\pm$ 2	90 $\pm$ 2	90 $\pm$ 1
2750	2766 $\pm$ 175	39.4 $\pm$ 0.6	1.00 $\pm$ 0.02	1.00 $\pm$ 0.02	90 $\pm$ 2	90 $\pm$ 2	90 $\pm$ 2
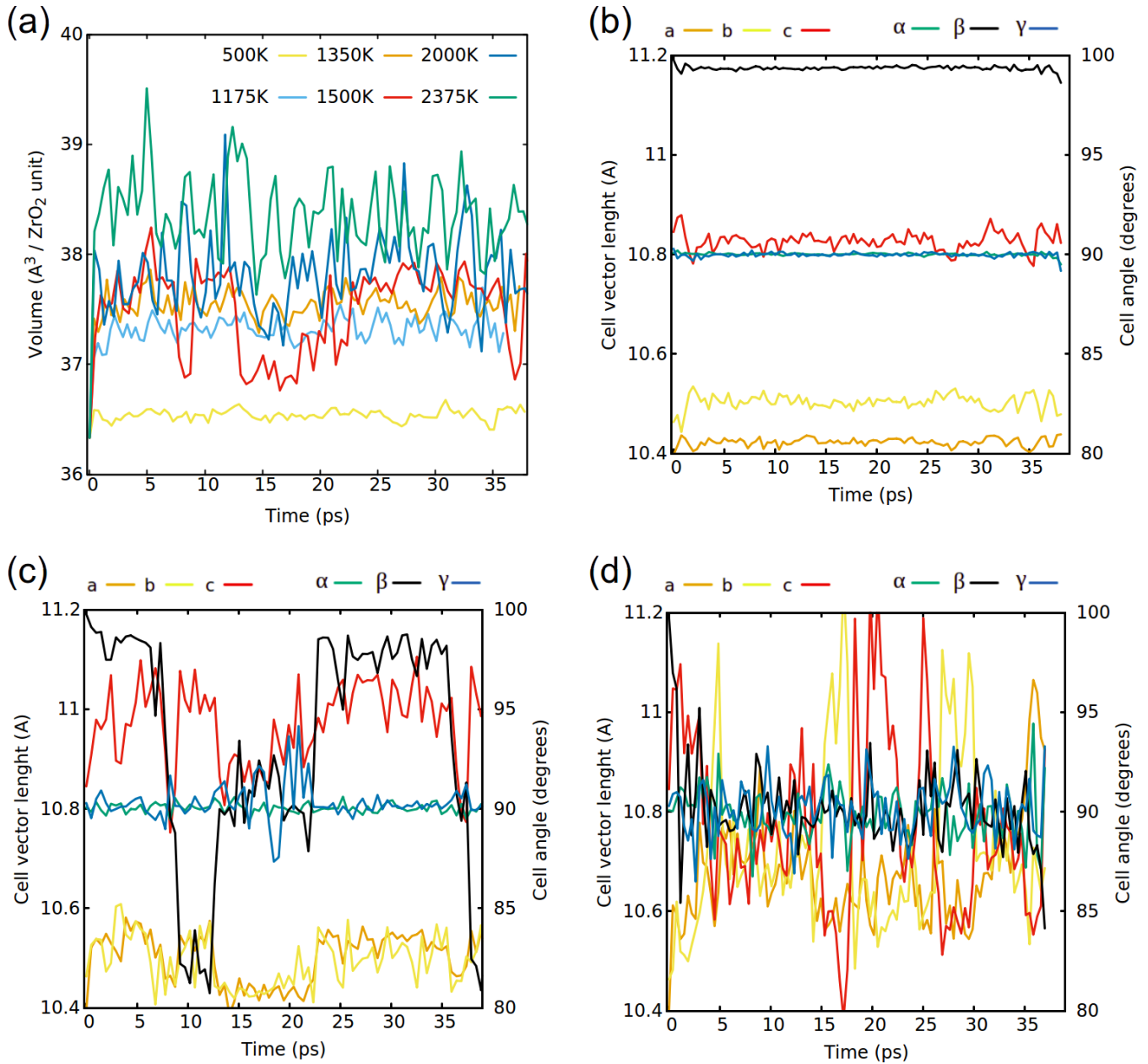
FIG. 4. Panel (a) shows the unit cell's volume as a function of the simulation time for different temperatures for the pristine ZrO_2 system. Panels (b)–(d) show the unit-cell parameters (vector lengths a, b, c and cell angles α, β, γ) as a function of time for 500, 1500, 2375 K, respectively. Every point represents an average calculated over 100 fs of evolution.

the temperature from 500 to 1350 K does not change the symmetry of the system, but causes a 3% volume expansion and a lattice change to $a \approx b$. Table I shows the average parameters obtained for each run.

The clear picture at $T \leqslant 1350$ K is quickly replaced by a more complex behavior at 1500 K [see Fig. 4(a)]. The volume fluctuations are much larger, and the reason is not only related to the higher kinetic energy of the system, since at 1350 K the available kinetic energy is nearly the same and the volume changes significantly smaller. To better understand this more complex pattern, we analyzed how the supercell's parameter changes during the run, shown in Fig. 4(c). One can see that the cell lengths have a $a \approx b < c$ pattern at all time steps, while $\alpha \approx \gamma \approx 90°$. The β angle, however, assumes three

distinct values, 82° or 98°, for large periods of time, or 90° in between the other two, for a shorter time. This is a signal of a MC $\rightarrow$ Tet phase transformation, since $\beta = 82°$ or 98° are supplementary angles typical of the monoclinic structure, and 90° is the straight angle of the tetragonal case. This transition is also confirmed by the pair distribution function shown in the supplemental material [37], where one can see an increase in the Zr-O coordination from seven to eight at typical first-neighbor distances between 3 and 3.5 Å for temperatures larger than 1500 K. Since the MC structure has a 0 K volume 5% larger than the Tet one, during this transition the volume changes are much larger, which explains the behavior obtained in Fig. 4(a). Therefore, different phases can be identified at 1500 K depending on the time window δt in which

the analysis is performed: a small δt value gives either a Tet or MC phase, information that is typically accessible through PDF (pair distribution function) measurements; a larger δt always gives a tetragonal phase with a $\beta \approx 91°$ and large deviations of $7°$ (see Table I).

We note here that, when different starting points are chosen instead of the equilibrium MC structure, the overall same structure and averages are obtained. Indeed, NPT-AIMD runs starting from Tet or Cub phases at representative 500 and 2000 K, shown in the supplemental material [37], give that about 10 ps are enough to stabilize the phase which is the most stable one at the current temperature, and the structural averages are already quite similar even if the system is not completely thermalized yet. This indicates that ensemble averages should be similar to time averages, given that the energy barrier connecting the different phases of zirconia is low and can be easily overcome at room temperature. The limited numerical accuracy of the methodology employed should also be highlighted a this point. Indeed, in an ideal NPT molecular-dynamics simulation, an infinite number of atoms in an infinitely long run would provide a system perfectly thermalized at the exact target temperature. In our work, our main numerical limitations are the 95-atom supercell and 25 ps thermalization time, which give only an average temperature that fluctuates about 100 K around the 1500 K target temperature (see Table I). Thus, instead of obtaining a single critical temperature, as typically obtained experimentally, our approach can accurately identify a temperature region where the transition occurs. With this in mind, we found out that the predicted MC $\to$ Tet temperature for pure zirconia, according to our calculations, falls inside the 1500 ± 100 K range, which is in very good agreement with the known experimental value of 1500 K.

Increasing the temperature further gives the complete stabilization of the Tet phase. Already at 1750 K, the average supercell parameters (Table I) give a Tet phase during the whole run. At 2350 K, however, a Tet $\to$ *Cub* transition start to occur. In Fig. 4(d) it can be seen that, while all three α, β, and γ angles are on average 90° (see Table I), the lattice lengths switch between $a = b < c$, $a = c < b$, and $b = c < a$. Again, an average in a large δt gives a cubic symmetry, even though the tetragonal phase is still the predominant phase during most of the run. At 2750 K only the cubic phase is obtained during the whole run, which gives that the Tet $\to$ Cub transition should occur between the 2350 K $< T < 2750$ K values. This is in good agreement with the known experimental value of 2700 K for this phase transition.

We conclude this kinetics study of pure zirconia highlighting the accuracy of the NPT-AIMD approach, which reproduces very well the expected temperature dependence of zirconia's distinct phases and also the intermediate transition regions. However, to be more quantitative, more target temperatures need to be considered, as will be done next for the more interesting Ti-doped 3YSZ material.

C. Kinetics of Ti-doped 3YSZ

Using the same procedure of the last section, we studied the Ti-doped 3YSZ system with 0%, 9%, and 19% Ti content at 15 different temperatures (see Computational Details).
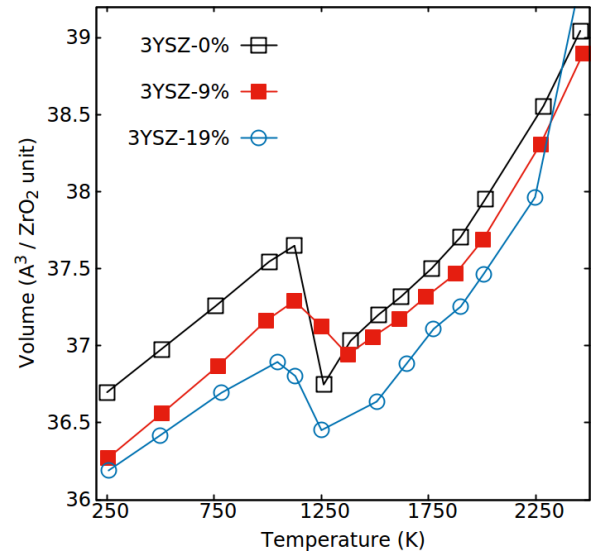

FIG. 5. Average unit-cell volume as a function of temperature for the Ti-doped 3YSZ system with Ti concentrations of 0%, 9%, and 19%.

Starting from the most stable structures illustrated in Fig. 1, we show in Fig. 5 the obtained average crystal volume as a function of temperature T in the 250 K $< T <$ 2450 K range. The general picture of the three curves is similar: a linear volume increase up to a temperature around 1000 K; a volume drop related to the MC $\to$ Tet transition, or Triclinic $\to$ Orthorhombic for the 19% Ti case; a second linear volume increase up to 2000 K, at least. There are, however, important differences between each Ti content, which are enumerated next.

1. The temperature in which the first transition occurs is similar for the three cases, but the temperature size window in which it occurs is different. Higher Ti compositions give "slower" transitions. This behavior is related to the lower energy differences between the MC and Tet or Orthorhombic phases at higher Ti compositions (see Fig. 3), which results in a coexistence of phases in a larger temperature range.

2. The magnitude of the volume decrease during the transition, for both 9% and 19% cases, is significantly smaller with respect to undoped 3YSZ. Therefore, the Ti-doped material is potentially more resistant to cracking. This result can also be related to recent experimental measurements by Zeng *et al.* [4] that showed that 3YSZ crystals doped with a small amount of Ti presented better shape memory properties.

3. The slope of the linear growth can be associated with the thermal expansion of each material. To quantify such a parameter, we evaluated the thermal-expansion coefficient α_L assuming an isotropic material, given by

$$\alpha_L(T) = \frac{1}{3V} \frac{\partial V}{\partial T} \, . \tag{1}$$

Since our main objective here is to investigate the changes in zirconia due to the Y-Ti codoping, we evaluated α_L only at 250 K, the temperature in which all structures have only a single phase, which is (near) monoclinic for all compositions. The results are shown in Table II, where it can be observed that doping zirconia with 3% yttria significantly increases

TABLE II. For zirconia and 3YSZ crystals with different Ti compositions, the isotropic thermal-expansion coefficient is shown, evaluated at 250 K using the data from Fig. 5, Table I and Eq. (1).

Material	α_L (10^{-6} K^{-1})
ZrO$_2$	7.3
Ti-0% 3YSZ	10.0
Ti-9% 3YSZ	10.5
Ti-19% 3YSZ	8.2

the α_L value. This result is in close agreement with typically reported experimental and theoretical values for pure zirconia and 3YSZ, with deviations of no more than 10% [41–45].

For the $X_{Ti} = 9\%$ case, there is only a small variation of α_L, indicating that small amounts of Ti leads to minimal changes in the overall initial response to heating, probably due to the localization around the oxygen vacancy for the added Ti, as opposed to forming extended TiO$_2$ rows. In contrast, the $X_{Ti} = 19\%$ case shows a large decrease in α_L, related to the already discussed larger competition between MC and Tet phases, which allows the system to better release the strain when heated.

4. At temperatures higher than 1500 K, a linear volume increase of the tetragonal or orthorhombic phases take place. For both $X_{Ti} = 0\%$ and $X_{Ti} = 9\%$, this increase is rather similar up to 2500 K. For $X_{Ti} = 19\%$, at $\approx$2000 K the linear
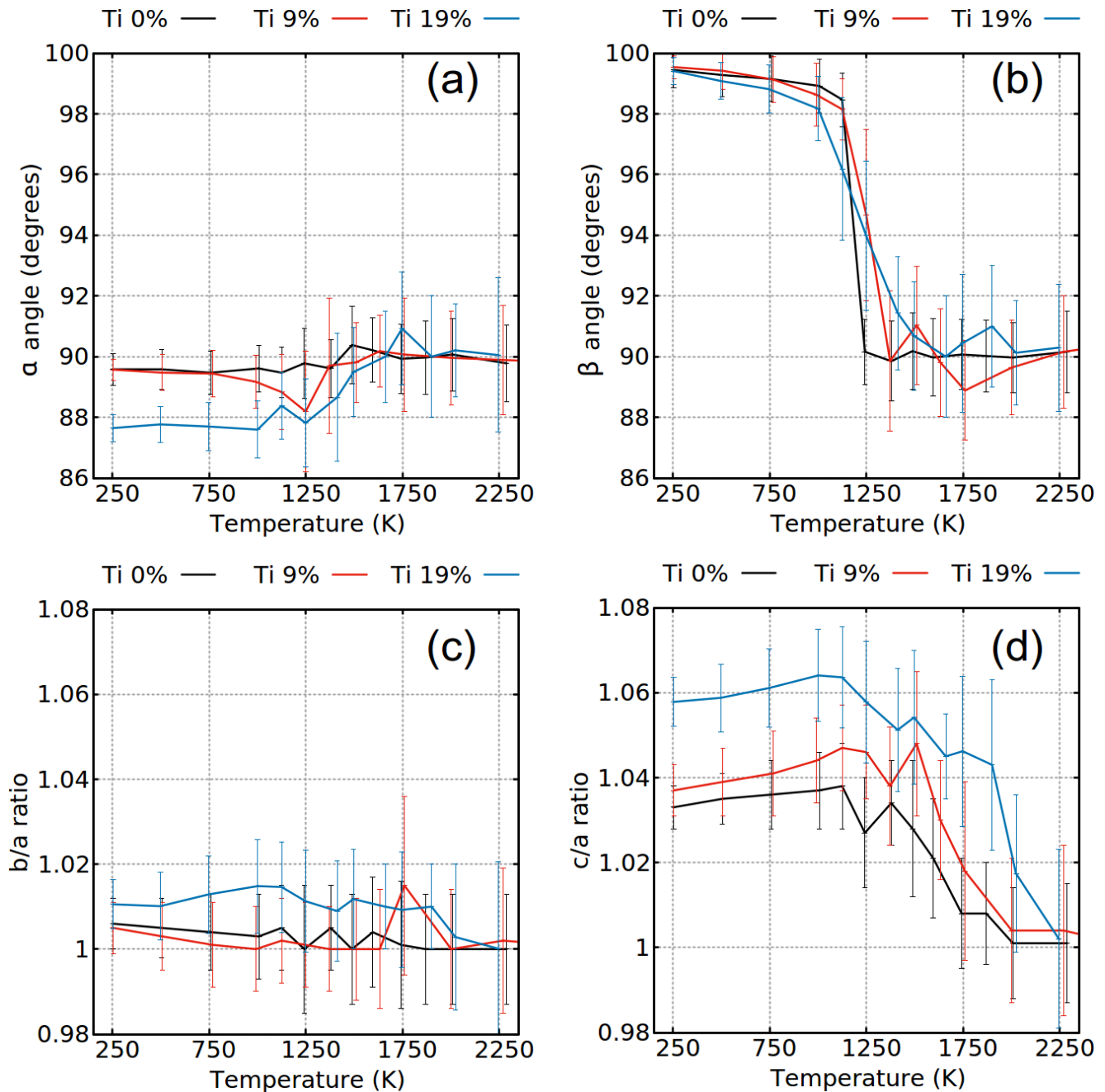

FIG. 6. For the 3YSZ structure with Ti contents of 0%, 9%, and 19%, the average (a) α and (b) β angles, and the (c) b/a and (d) c/a ratio are shown as a function of temperature.

increase is replaced by a much higher exponential-like increase, related to the melting of the material. This reduction of the melting point due to Ti doping is expected, given that, in the TiO_2/ZrO_2 phase diagram, the melting point reduces linearly by about 100 K for each 10% of Ti doping [6]. We highlight, however, that the decrease obtained is not linear due to the strong interaction between Ti and the oxygen vacancy.

The Tet → Cub transition is not very clear looking only in Fig. 5, considering the small volume difference between these two phases and their similar thermal expansion. This transition is better identified by analyzing each lattice vector variation with temperature. This is shown in Fig. 6, where the average α and β angles, together with the b/a and c/a ratio at each X_{Ti} are plotted. We note that the average value of the γ angle is very close to 90° in all cases, and therefore is not shown. Figure 6 reveals much more clearly both phase-transition regions. The 0% and 9% cases show, at 500 K, a transition from MC with $a < b$ to MC with $a = b$; MC → Tet at around 1300 K; a Tet → Cub phase starting around 2000 K. For $X_{Ti} = 19\%$, the structure is triclinic at low temperatures, as it is at 0 K (see Fig. 2), since $\alpha \approx 87.5°$ and $\beta \approx 99.5°$. At 1125 K a transition to orthorhombic takes place, ending at ≈1500 K, and at $T > 2000$ K an average cubic phase can be identified, even though the deviations become significantly large at this temperature. Therefore, an average cubic phase can be identified for all Ti contents, but only at temperatures larger than 2000 K.

A quick visualization on how the atoms move during the simulation also reveals that, although no diffusion of Zr, Ti, or Y is seen even at temperatures as high as 2000 K (as shown in the supplemental material [37]) oxygen diffusion occurs quite often. This is expected since 40 ps is a short time to view processes with high energy barriers (higher than 1 eV), while it is enough to view fast processes that occur with a frequency of the order of ps^{-1}. To quantify the O diffusion frequency, the number of oxygen site-jumps was counted for a few representative temperatures, and the result is shown in Fig. 7. While for pure ZrO_2 crystals O diffusion only occurs at temperatures around 2000 K, it already starts at 1250 K for 3YSZ crystals, and 1375 K for the 9% and 19% Ti-doped cases. This is also confirmed by evaluating the average oxygen displacement, as shown in the supplemental material [37]. Yttria doping in zirconia is known to increase O diffusion, given the addition of oxygen vacancies [46–48]. Ti doping, on the other hand, is shown here to increase the energy barrier for oxygen diffusion, starting at a temperature around 100 K higher. This is connected to the stronger interaction between the Ti atoms and the oxygen vacancy that somewhat blocks the O vacancy. However, Ti doping also significantly increases the diffusion frequency once this barrier is overcome, with a very similar magnitude for both 9% and 19% cases. We further note that, since O diffusion is a fast process at large temperatures, other structural configurations with different degrees of interaction between the O vacancy and the Zr or Ti atoms were explored during the NPT-AIMD runs. So although the kinetic results presented are restricted by the initial chemical configuration, chosen to be the 0 K global minimum, a considerable large part of the potential-energy surface was sampled during the dynamics.
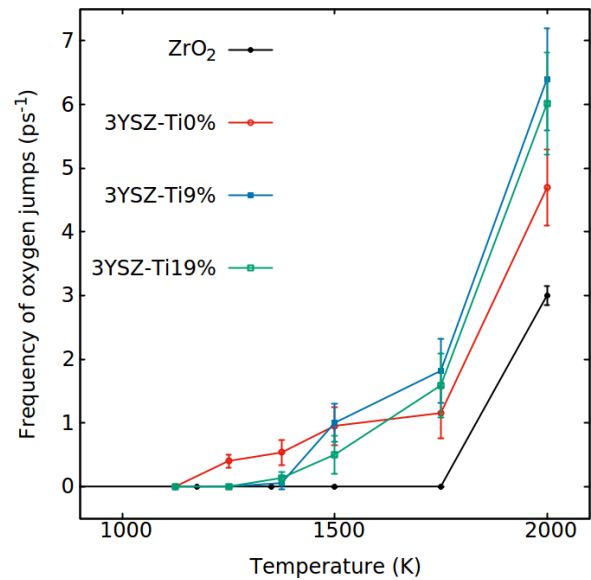

FIG. 7. Frequency of oxygen diffusion as a function of temperature for different materials.

The results presented here indicate that 9% of Ti doping does not change significantly some properties of the 3YSZ material, such as melting point and thermal expansion. However, it does improve its response to thermal cracking and also shows a negative formation energy (Fig. 2), i.e., it is thermodynamically more stable than the undoped 3YSZ. Further doping up to 19% changes most of the material properties due to the formation of TiO_2 channels inside the 3YSZ, which decreases significantly its melting point and reduces its thermodynamic stability. So the 9% amount is potentially ideal to optimize the overall stability of the material. Since this composition is chemically characterized by oxygen vacancy defects surrounded by Ti, and the amount of oxygen vacancies is related to Y doping, we can hypothesize that the general optimal amount of Ti in a YSZ material is directly related to the amount of Y doping, in the optimal proportion of 1% of Y_2O_3 for every 3% TiO_2, an extrapolation that should be valid in the regime of low Y or Ti content, at least.

IV. CONCLUSIONS

The effects of Ti doping on 3%-yttria-doped zirconia crystals (3YSZ) were studied at the DFT level, with special focus on the stability of its most stable monoclinic, tetragonal, and cubic phases. The methodology applied consisted in performing a global search analysis to explore the potential-energy surface at 0 K, followed by *ab initio* molecular dynamics to evaluate the kinetic properties of the material at higher temperatures. The simulations accurately provided the material's volume dependence with temperature and Ti content, together with the temperature range where each phase is more stable. A detailed atomistic description of the phase-transition regions was also provided, providing a support and increasing the understanding of the experimental and theoretical data that can be found in the literature.

The basin hopping global search algorithm was initially used to determine the most stable sites for Ti doping in the 3YSZ structure as a function of the Ti composition (X_{Ti}), which were found to be initially around the oxygen vacancy, completely surrounding it at $X_{Ti} = 9\%$. Further addition of Ti gives the appearance of infinite Ti channels in the system, and eventually complete TiO_2 planes. The formation energy as a function of X_{Ti} presents an energy minimum at $X_{Ti} = 9\%$, with the added Ti atoms stabilizing the under-coordinated cation sites first neighbor to the oxygen vacancy. Indeed, after these sites are filled with Ti, further Ti doping only increase the formation energy of the system, until it eventually becomes positive at $X_{Ti} > 22\%$, where phase separation or a new phase is expected to form.

AIMD runs within the NPT ensemble further revealed that Ti doping causes a significant reduction in the volume change during the MC → Tet transition, which indicates that the Ti-doped materials have a much higher resistance to cracking than the pure zirconia and yttria-stabilized counterparts. Therefore, the combined thermodynamic and kinetic studies suggest that the 9% Ti-doped 3YSZ material has an overall higher stability. Since the better stability is related to the amount of oxygen vacancies in the system, which in turn is associated with the amount of Y doping, we hypothesize that there is, in fact, an optimal proportion of Y-Ti codoping in zirconia, which is $3TiO_2$ units for each Y_2O_3 one.

ACKNOWLEDGMENTS

[1] P. Ducheyne, D. W. Grainger, K. E. Healy, D. W. Hutmacher, and C. J. Kirkpatrick, *Comprehensive Biomaterials II* (Elsevier, Amsterdam, Netherlands, 2017).

[2] J. A. Krogstad, M. Lepple, Y. Gao, D. M. Lipkin, and C. G. Levi, Effect of yttria content on the zirconia unit cell parameters, J. Am. Ceram. Soc. **94**, 4548 (2011).

[3] U. Troitzsch, TiO_2-doped zirconia: Crystal structure, monoclinic-tetragonal phase transition, and the new tetragonal compound Zr_3TiO_8, J. Am. Ceram. Soc. **89**, 3201 (2006).

[4] X. M. Zeng, Z. Du, C. A. Schuh, N. Tamura, and C. L. Gan, Microstructure, crystallization and shape memory behavior of titania and yttria co-doped zirconia, J. Eur. Ceram. Soc. **36**, 1277 (2016).

[5] R. De Paula, W. Miranda, D. Lazar, V. Ussui, J. Marchi, and P. Cesar, Effect of titania content and biomimetic coating on the mechanical properties of the Y-TZP/TiO_2 composite, Dent. Mater. **34**, 238 (2017).

[6] T. A. Schaedler, O. Fabrichnaya, and C. G. Levi, Phase equilibria in the $TiO_2 - YO_{1.5}$-ZrO_2 system, J. Eur. Ceram. Soc. **28**, 2509 (2008).

[7] M. Colomer, Straightforward synthesis of Ti-doped YSZ gels by chemical modification of the precursors alkoxides, J. Sol-Gel Sci. Technol. **67**, 135 (2013).

[8] M. Mori, Y. Hiei, H. Itoh, G. A. Tompsett, and N. M. Sammes, Evaluation of Ni and Ti-doped Y_2O_3 stabilized ZrO_2 cermet as an anode in high-temperature solid oxide fuel cells, Solid State Ionics **160**, 1 (2003).

[9] M. Zhao and W. Pan, Effect of lattice defects on thermal conductivity of Ti-doped, Y_2O_3-stabilized ZrO_2, Acta Mater. **61**, 5496 (2013).

[10] F. Gallino, C. Di Valentin, and G. Pacchioni, Band gap engineering of bulk ZrO_2 by Ti doping, Phys. Chem. Chem. Phys. **13**, 17667 (2011).

[11] H. Chauke, R. Grau-Crespo, P. Ngoepe, and N. Leeuw, Theoretical investigation of Ti-doped zirconia surfaces, J. Phys. Chem. C **114**, 15403 (2010).

[12] P. Hohenberg and W. Kohn, Inhomogeneous electron gas, Phys. Rev. **136**, B864 (1964).

[13] M. A. Zaeem, N. Zhang, and M. Mamivand, A review of computational modeling techniques in study and design of shape memory ceramics, Comput. Mater. Sci. **160**, 120 (2019).

[14] H. Ding, A. V. Virkar, and F. Liu, Defect configuration and phase stability of cubic versus tetragonal yttria-stabilized zirconia, Solid State Ionics **215**, 16 (2012).

[15] A. Predith, G. Ceder, C. Wolverton, K. A. Persson, and T. Mueller, *Ab initio* prediction of ordered ground-state structures in ZrO_2-Y_2O_3, Phys. Rev. B **77**, 144104 (2008).

[16] D. Sangalli and A. Debernardi, Exchange-correlation effects in the monoclinic to tetragonal phase stabilization of yttrium-doped ZrO_2: A first-principles approach, Phys. Rev. B **84**, 214113 (2011).

[17] R. Terki, G. Bertrand, H. Aourag, and C. Coddet, Structural and electronic properties of zirconia phases: A FP-LAPW investigations, Mater. Sci. Semicond. Process. **9**, 1006 (2006).

[18] A. G. Gebresilassie, Atomic scale simulations in zirconia: Effect of yttria doping and environment on stability of phases, Ph.D. thesis, Université de Lyon, 2016 (unpublished).

[19] G. Cousland, X. Cui, S. Ringer, A. Smith, A. Stampfl, and C. Stampfl, Electronic and vibrational properties of yttria-stabilised zirconia from first-principles for 10–40 mol% Y_2O_3, J. Phys. Chem. Solids **75**, 1252 (2014).

[20] C. Carbogno, C. G. Levi, C. G. Van de Walle, and M. Scheffler, Ferroelastic switching of doped zirconia: Modeling and understanding from first principles, Phys. Rev. B **90**, 144109 (2014).

[21] G. Jomard, T. Petit, A. Pasturel, L. Magaud, G. Kresse, and J. Hafner, First-principles calculations to describe zirconia pseudopolymorphs, Phys. Rev. B **59**, 4044 (1999).

[22] G. Cousland, X. Y. Cui, A. Smith, A. P. Stampfl, and C. Stampfl, Mechanical properties of zirconia, doped and undoped yttria-stabilized cubic zirconia from first-principles, J. Phys. Chem. Solids **122**, 51 (2018).

[23] C. Gehrmann and D. A. Egger, Dynamic shortening of disorder potentials in anharmonic halide perovskites, Nat. Commun. **10**, 3141 (2019).

[24] A. V. Cohen, D. A. Egger, A. M. Rappe, and L. Kronik, Breakdown of the static picture of defect energetics in halide

perovskites: The case of the Br vacancy in CsPbBr$_3$, J. Phys. Chem. Lett. **10**, 4490 (2019).

[25] X. Zhao, G. M. Dalpian, Z. Wang, and A. Zunger, Polymorphous nature of cubic halide perovskites, Phys. Rev. B **101**, 155137 (2020).

[26] R. X. Yang, J. M. Skelton, E. L. da Silva, J. M. Frost, and A. Walsh, Assessment of dynamic structural instabilities across 24 cubic inorganic halide perovskites, J. Chem. Phys. **152**, 024703 (2020).

[27] J. P. Perdew, K. Burke, and M. Ernzerhof, Generalized Gradient Approximation made Simple, Phys. Rev. Lett. **77**, 3865 (1996).

[28] J. Hutter, M. Iannuzzi, F. Schiffmann, and J. VandeVondele, CP2K: Atomistic simulations of condensed matter systems, Wiley Interdiscip. Rev. Comput. Mol. Sci. **4**, 15 (2014).

[29] S. Goedecker, M. Teter, and J. Hutter, Separable dual-space Gaussian pseudopotentials, Phys. Rev. B **54**, 1703 (1996).

[30] C. Hartwigsen, S. Goedecker, and J. Hutter, Relativistic separable dual-space Gaussian pseudopotentials from H to Rn, Phys. Rev. B **58**, 3641 (1998).

[31] M. Krack, Pseudopotentials for H to Kr optimized for gradient-corrected exchange-correlation functionals, Theor. Chem. Acta **114**, 145 (2005).

[32] J. VandeVondele and J. Hutter, Gaussian basis sets for accurate calculations on molecular systems in gas and condensed phases, J. Chem. Phys. **127**, 114105 (2007).

[33] P. Giannozzi, S. Baroni, N. Bonini, M. Calandra, R. Car, C. Cavazzoni, D. Ceresoli, G. L. Chiarotti, M. Cococcioni, I. Dabo *et al.*, Quantum espresso: A modular and open-source software project for quantum simulations of materials, J. Phys.: Condens. Matter **21**, 395502 (2009).

[34] K. F. Garrity, J. W. Bennett, K. M. Rabe, and D. Vanderbilt, Pseudopotentials for high-throughput DFT calculations, Comput. Mater. Sci. **81**, 446 (2014).

[35] J. H. Monkhorst and D. J. Pack, Special points for Brillouin-zone integrations, Phys. Rev. B **13**, 5188 (1976).

[36] D. J. Wales, and H. A. Scheraga, Global optimization of clusters, crystals, and biomolecules, Science **285**, 1368 (1999).

[37] See Supplemental Material at http://link.aps.org/supplemental/10.1103/PhysRevMaterials.5.023603 for structural view, energy differences, and volume of several different chemical compositions for the 12%-Ti-doped 3YSZ; total energy curves and pressure as a function of the simulation time at different temperatures; integrated pair distribution function for

Zr-O bonds; AIMD simulations starting from the cubic and tetragonal phases; average atomic displacement as a function of temperature for pure zirconia, 3YSZ and Ti-doped 3YSZ. In addition, the CP2K and QE inputs used are given with the optimized coordinates of each global minima found.

[38] X. Miao, D. Sun, P. W. Hoo, J. Liu, Y. Hu, and Y. Chen, Effect of titania addition on yttria-stabilised tetragonal zirconia ceramics sintered at high temperatures, Ceram. Int. **30**, 1041 (2004).

[39] O. Fabrichnaya and F. Aldinger, Assessment of the thermodynamic parameters in the system ZrO$_2$-Y$_2$O$_3$-Al$_2$O$_3$, Z. Metallkd. **95**, 27 (2004).

[40] S. Fabris, A. T. Paxton, and M. W. Finnis, Free energy and molecular dynamics calculations for the cubic-tetragonal phase transition in zirconia, Phys. Rev. B **63**, 094101 (2001).

[41] L. Jin, L. Ni, Q. Yu, A. Rauf, and C. Zhou, Theoretical calculations of thermodynamic properties of tetragonal ZrO$_2$, Comput. Mater. Sci. **65**, 170 (2012).

[42] V. Petukhov, Thermal expansion of zirconium in the solid phase, High Temperatures-High Pressure **35/36**, 15 (2003).

[43] H. Schubert, Anisotropic thermal expansion coefficients of Y$_2$O$_3$-stabilized tetragonal zirconia, J. Am. Ceram. Soc. **69**, 270 (1986).

[44] G. B. Skinner and H. L. Johnston, Thermal expansion of zirconium between 298°K and 1600°K, J. Chem. Phys. **21**, 1383 (1953).

[45] H. Hayashi, T. Saitou, N. Maruyama, H. Inaba, K. Kawamura, and M. Mori, Thermal expansion coefficient of yttria stabilized zirconia for various yttria contents, Solid State Ionics **176**, 613 (2005).

[46] M. Kilo, C. Argirusis, G. Borchardt, and R. A. Jackson, Oxygen diffusion in yttria stabilised zirconia-experimental results and molecular dynamics calculations, Phys. Chem. Chem. Phys. **5**, 2219 (2003).

[47] R. Krishnamurthy, Y. Yoon, D. Srolovitz, and R. Car, Oxygen diffusion in yttria-stabilized zirconia: A new simulation model, J. Am. Ceram. Soc. **87**, 1821 (2005).

[48] A. V. Yakimov, D. O. Filatov, O. N. Gorshkov, D. A. Antonov, D. A. Liskin, I. N. Antonov, A. V. Belyakov, A. V. Klyuev, A. Carollo, and B. Spagnolo, Measurement of the activation energies of oxygen ion diffusion in yttria stabilized zirconia by flicker noise spectroscopy, Appl. Phys. Lett. **114**, 253506 (2019).